Applied Catalysis B: Environmental 245 (2019) 681–690

Contents lists available at ScienceDirect

Applied Catalysis B: Environmental

journal homepage: www.elsevier.com/locate/apcatb

Development of visible-light-responsive morphology-controlled brookite TiO_2 nanorods by site-selective loading of AuAg bimetallic nanoparticles

Ying Ma[a], Katsuichiro Kobayashi[a], Yu Cao[a], Teruhisa Ohno[a,b,*]

[a] Department of Materials Science, Faculty of Engineering, Kyushu Institute of Technology, 1-1 Sensui-cho, Tobata-ku Fukuoka, Kitakyushu, 804-8550, Japan
[b] Research Center for Solar Light Energy Conversion, 1-1 Sensuicho, Tobata, Kitakyushu, 804-8550, Japan

ARTICLE INFO

Keywords:
Brookite
Surface plasmon resonance
AuAg bimetallic
Visible-light-responsive
Photocatalytic

ABSTRACT

Morphology-controlled brookite TiO_2 nanorods loaded with AuAg bimetallic nanoparticles were synthesized by a facile photoreduction process to develop visible-light-responsive photocatalytic performance. The AuAg bimetallic nanoparticles provide good stability and excellent localized surface plasmon resonance (LSPR) effect. Moreover, the AuAg bimetallic nanoparticles were selectively deposited on the reduction facets of brookite TiO_2 nanorods, facilitating the charge separation. As expected, the as-prepared AuAg-TiO_2 nanorods showed enhanced visible light harvesting and decreased electron-hole recombination, resulting in superior visible-light-responsive photocatalytic performance. When the loading amount of AuAg nanoparticles was controlled at 0.5 wt%, the AuAg-TiO_2 nanorods yield 102 ppm acetone with visible-light irradiation for 5 h, far exceeding than those of bare brookite TiO_2 nanorods.

1. Introduction

Photocatalysts, especially titanium dioxide (TiO_2), have been extensively studied as promising materials for water splitting and decomposition of organic pollutants by using solar energy. TiO_2 typically exists as three types of polymorphs: anatase, rutile and brookite [1–3]. With the recent development of improved methods for synthesis of brookite TiO_2, many investigations of its photocatalytic properties have been carried out. It has been shown that brookite TiO_2 is superior for photocatalytic reactions than those of anatase and rutile due to the appropriate depth of electron traps, which greatly benefits the overall photocatalytic activity [4–6]. However, the photoabsorption of brookite TiO_2 is limited to UV light as is rutile TiO_2 and anatase TiO_2, which greatly hinders the utilization of solar energy and practical applications in photocatalytic decompositions especially indoors [7]. Therefore, it is critical to develop the visible-light response of brookite TiO_2 for photocatalysis by enhancing its ability to absorb and harvest visible light.

Surface plasmon resonances of metallic nanoparticles provide an efficient strategy for obtaining advanced photovoltaic and photocatalytic devices. As the most important and common co-catalysts, Ag and Au have been studied extensively because of their LSPR effect on semiconductor photocatalysts, which could not only promote visible light absorption but also charge separation. For instance, an Ag-TiO_2 composite catalyst [8], Ag@TiO_2 nanorods [9], Au-TiO_2 [10] and Ag-TiO_2 plasmonic hybrid nanocomposites [11] have been prepared and shown greatly enhanced visible-light-responsive photocatalytic performance. However, pure Au nanoparticles exhibit low LSPR effect and Ag nanoparticles demonstrate poor stability under visible light. Hence, AuAg bimetallic nanoparticles attracted much attention due to the synergistic effect of Ag and Au, enabling good stability and excellent LSPR effect. Tahir et al. reported a synergistic effect of plasmonic Au/Ag alloy nanoparticles used for coating TiO_2 nanowires on visible-light-promoted photoreduction of CO_2 to fuels [12]. Huang's group validated the superiority of gold-silver-modified plasmonic photoanodes for solar cells with high efficiency under visible light [13]. Therefore, it is highly desirable to investigate the LSPR effect of AuAg bimetallic nanoparticles on brookite TiO_2, developing efficient visible-light-driven photocatalyst.

In this study, well-defined AuAg-brookite TiO_2 nanorods were fabricated by selectively loading AuAg bimetallic nanoparticles on morphology-controlled brookite TiO_2 nanorods. The efficient LSPR effect of AuAg nanoparticles on reduction facets of brookite TiO_2 nanorods remarkably enhanced visible-light absorption and charge separation, thus improving visible-light-driven photocatalytic performance. The combination of Au and Ag enables not only superior LSPR activity but also good stability, making it an ideal material for modifying brookite TiO_2 nanorods. Furthermore, 0.5 wt% AuAg-brookite showed high level of acetone production for decomposition of 2-propnal under visible light

* Corresponding author at: Department of Materials Science, Faculty of Engineering, Kyushu Institute of Technology, 1-1 Sensui-cho, Tobata-ku Fukuoka, Kitakyushu, 804-8550, Japan.
E-mail address: tohno@che.kyutech.ac.jp (T. Ohno).

https://doi.org/10.1016/j.apcatb.2019.01.016
Received 17 October 2018; Received in revised form 18 December 2018; Accepted 6 January 2019
Available online 16 January 2019
0926-3373/

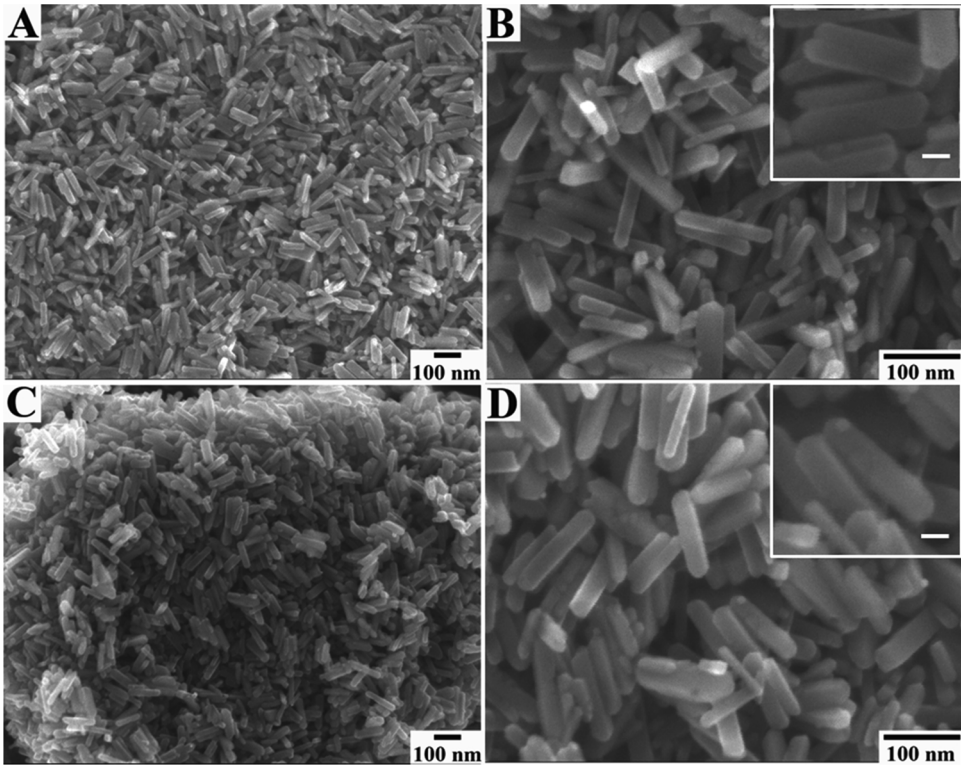

Fig. 1. SEM images of (A, B) pristine brookite TiO_2 (C, D) 0.5 wt% AuAg-TiO_2 nanorods. (The inset graphs are the corresponding enlarged SEM images and the scale bar represents 20 nm).

illumination, which is about 3 and 4 times of those of 0.5 wt% Ag-TiO_2 and 0.5 wt% Au-TiO_2. The results of this study provide insights for the development of efficient visible-light-responsive photocatalytic performance of brookite TiO_2 nanorods by introducing the LSPR effect of AuAg bimetallic nanoparticles.

2. Experimental section

2.1. Preparation of brookite TiO_2 nanorods

All of the chemical materials used in this study were analytical grade and used without further purification. The resistivity of the deionized water used in all of the reactions was 18.25 MΩ cm. Brookite TiO_2 nanorods were prepared through a facial hydrothermal reaction according to a reported method [14]. Urea (21.02 *g*) was dissolved in titanium bis(ammonium lactate) dihydroxide (TALH, 5 mL) and deionized water (45 mL) with stirring for 2 h. Then the uniform mixed solution was transferred into a Teflon cup and kept at 200 °C for 48 h. When the autoclave had cooled down to room temperature, the samples were collected by centrifugation until the ionic strength of the filtrate was less than 10 μs cm^{-1}. Finally, pure brookite TiO_2 nanorods could be obtained by drying at 60 °C for 4 h in a vacuum oven. To remove the organic compounds that may have remained or had been adsorbed on the surface of brookite TiO_2 nanorods, the products were irradiated with a 500 W mercury lamp (Ushio, SX-UI501UO) for 24 h. Commercial brookite TiO_2 was purchased from High Purity Materials Kojundo Chemical Laboratory Co. LTD.

2.2. Fabrication of AgAu/TiO_2 nanorods

AgAu bimetallic nanoparticles were loaded on the as-prepared brookite TiO_2 nanorods through a photo-reduction method. Firstly, 0.4 g brookite TiO_2 nanorod was dispersed in distilled water (10 mL) and methanol (10 mL). Then the mixed solution was bubbled with nitrogen for 1 h and irradiated with UV light (220 mW cm^{-2}). During the irradiation, 0.05 M silver nitrate was added at first. After 15 min, 0.029 M $HAuCl_4$ was added to the solution and its addition was repeated for 4 times. In order to control the loading amount of Au and Ag, the volume of added solution was regulated. More specifically, the loading amount of AuAg was confined to 0.25 wt%, 0.5 wt%, 0.75 wt% and 1.0 wt%, in which the molar ratio of Au and Ag is 1:1. For comparison, 0.5 wt% AgAu nanoparticles was also loaded on commercial brookite TiO_2 by the same procedure.

2.3. Characterization

The crystalline phase of as-prepared samples was investigated by using a powder X-ray diffraction (XRD) instrument (MiniFlex II, Rigaku Co.). The morphologies and nanostructures of the samples were characterized by using a scanning electron microscope (SEM, JSM-6701FONO) and a transmission electron microscope (TEM, Hitachi, H-9000NAR, 200 kV). High-resolution TEM (HRTEM) images were obtained through a Tecnai G2 F30 S-TWIN (30 kV). The surface area of the samples were obtained from a Quantachrome Nova 4200e using the Brunauer-Emmett-Teller (BET) and Barrett-Joyner-Halenda (BJH) methods, respectively. UV–vis diffuse reflectance spectra showing the optical properties of samples were obtained by a UV-2500PC (Shimadzu) equipped with an integrating sphere unit. X-ray photoelectron spectra (XPS) were obtained by a Thermo ESCALAB 250Xi system at room temperature using Al Kα with monochromatic radiation. Apparent quantum efficiency (AQE) at wavelengths from 400 to 600 nm was recorded by the ratio of acetone production and amount of incident photons by using a Xe lamp equipped with a band-pass filter (Asahi Spectra Co., Ltd.) centered at 400 nm, 450 nm, 470 nm, 500 nm, 550 nm and 600 nm. Photoluminescence (PL) spectra were characterized by the PF-8500 spectrometer using the excitation wavelength of 350 nm.

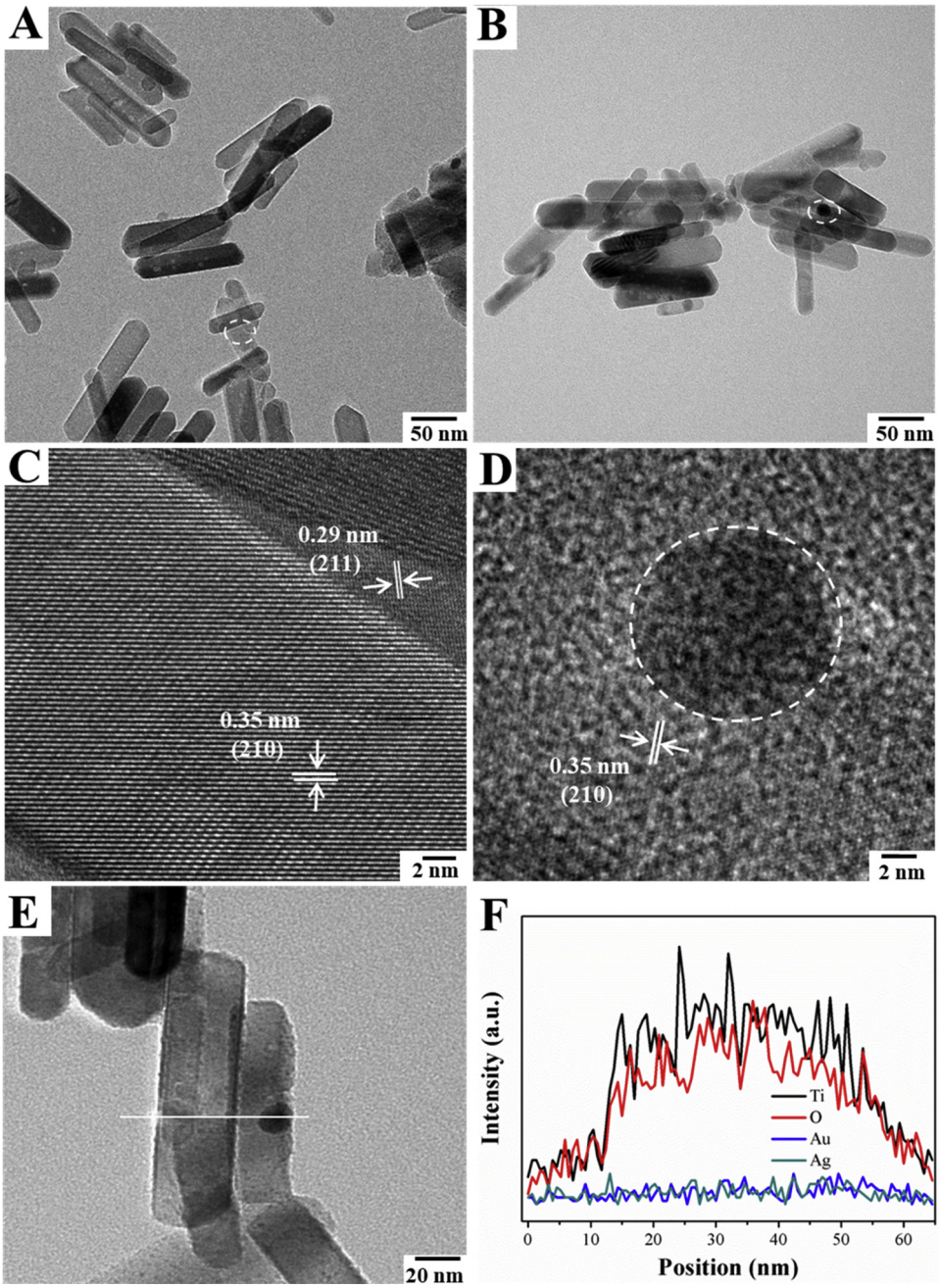

Fig. 2. TEM images of (A) pristine brookite TiO_2 and (B) 0.5 wt% AuAg-TiO_2 nanorods, HRTEM images of (C) pristine brookite TiO_2 and (D) 0.5 wt% AuAg-TiO_2 nanorods, (E) TEM image and (F) the corresponding line-scan electron energy loss spectroscopy (EELS) of 0.5 wt% AuAg-TiO_2 nanorods.

2.4. Photocatalytic test

The photocatalytic activity of the samples was evaluated by decomposition of 2-propanol in gas phase. The photocatalyst (200 mg) was spread on a glass dish (4 cm^2) and the glass dish was put into a Tedlar bag (AS ONE Co. Ltd.) with a volume of 125 mL mixed air (79% N_2, 21% O_2, < 0.1 ppm of CO_2, 500 ppm of 2-propanol). Before visible-light irradiation, the photocatalyst was left in the dark for 1 h to reach adsorption equilibrium. Then the photocatalyst was illuminated by visible light of 100 mW cm^{-2} (or 50 mW cm^{-2}) from a Xenon lamp equipped with a Yellow-44 filter. The concentration evolutions of 2-propanol, CO_2 and acetone during the photocatalytic process were determined by gas chromatography (Agilent/Inficon 3000 Micro GC) with a PLOT U column and OV-1 column.

3. Results and discussion

The nanorod shape of brookite TiO_2 is shown by SEM images in Fig. 1. It can be clearly seen that ordered nanorods with lengths of about 110 nm and widths of 20 nm have smooth surfaces and triangular-like tips at the ends of the rods (Fig. 1B). As reported previously, a nanorod shows a large {210} crystal face and a small {212} crystal face in the flank and top of brookite TiO_2, corresponding to reduction and oxidation facets, respectively [15,16]. Moreover, the large proportion of reduction sites in as-prepared brookite TiO_2 provides numerous active sites for photoreduction. As expected, the nanorod shape was preserved well and there were few nanoparticles distributed on the reduction facets of brookite TiO_2 nanorods after loading the AuAg nanoparticles as shown in Fig. 1D.

The TEM images in Fig. 2 show the specific morphology of pure

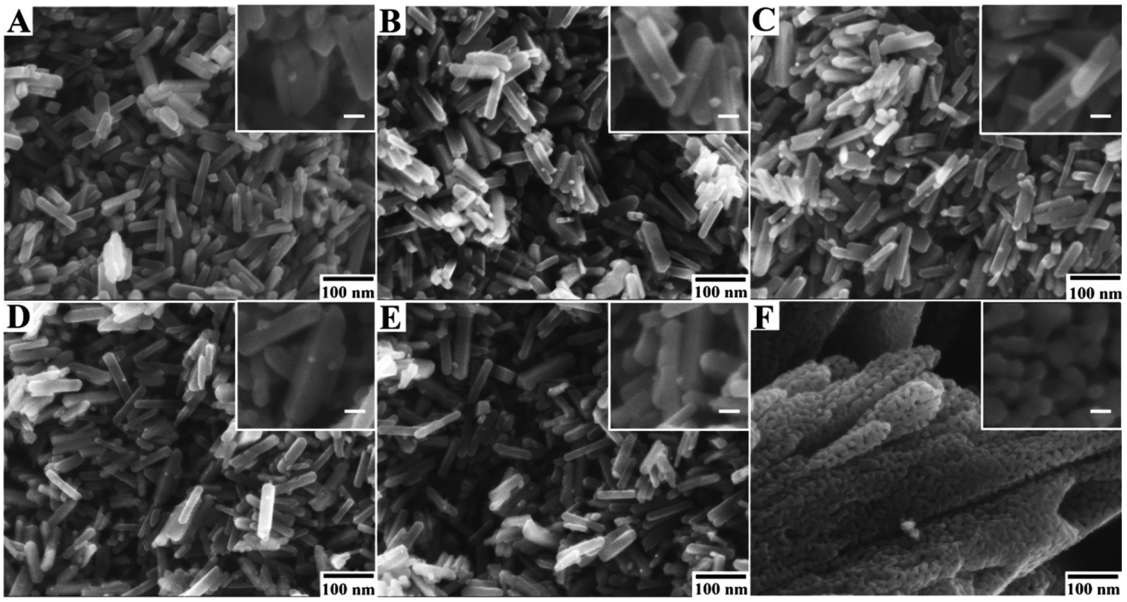

Fig. 3. SEM images of (A) 0.25 wt% AuAg-TiO_2 nanorods (B) 0.75 wt% AuAg-TiO_2 nanorods (C) 1.0 wt% AuAg-TiO_2 nanorods (D) 0.5 wt% Au-TiO_2 nanorods (E) 0.5 wt% Ag-TiO_2 nanorods (F) commercial brookite. (The inset graphs are the corresponding enlarged SEM images and the scale bar represents 20 nm).

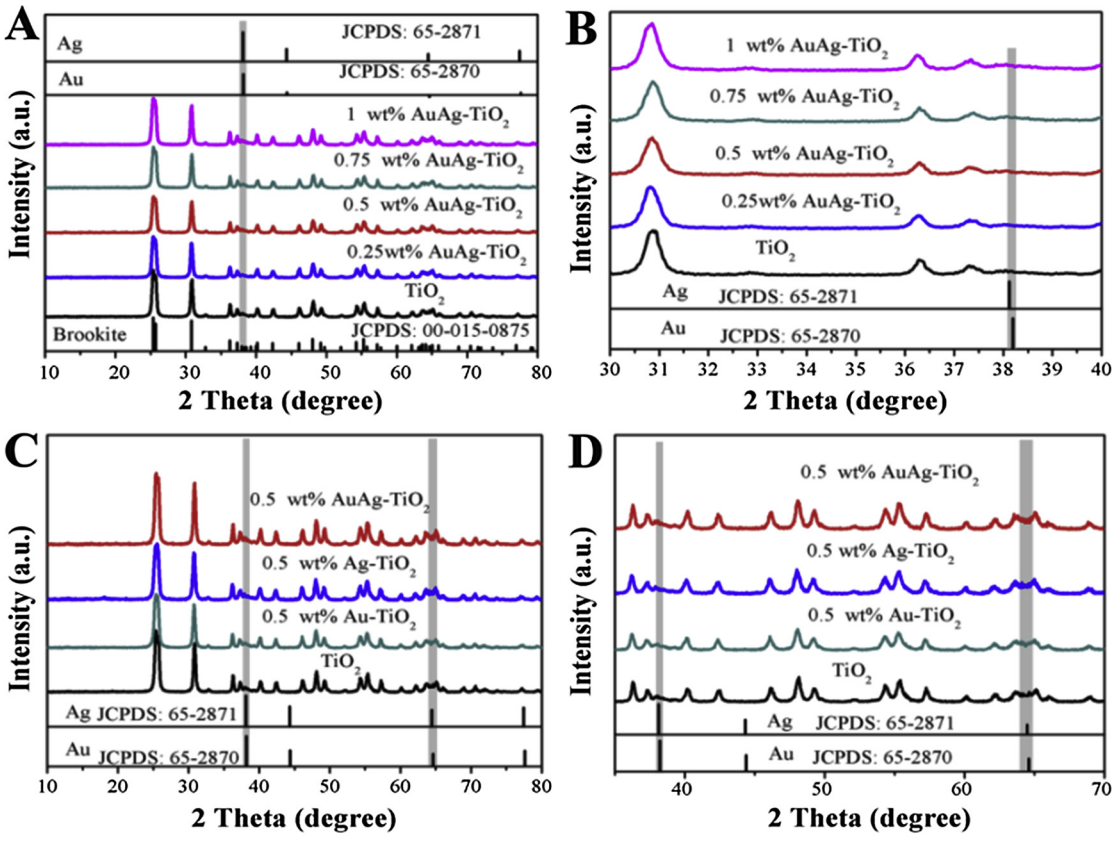

Fig. 4. XRD patterns (A and B) of AuAg-TiO_2 with different loading amounts of AuAg and XRD patterns (C and D) of brookite TiO_2 loaded with 0.5 wt% of different metals.

brookite TiO_2 nanorods and the existence of nanoparticles in the modified brookite TiO_2 nanorods. The TEM image of samples shows a rod-like shape with a triangular end and a tetragonal brookite structure, being consistent with the SEM images. The spacing lattices of 0.35 nm and 0.29 nm in HRTEM image derived from the bare nanorods marked with dotted line circle in TEM image can be assigned to the (210) and (211) facets of brookite TiO_2, which are identified as the reduction and oxidation facets [14,15]. Most importantly, nanoparticles (marked with dotted line circle in Fig. 2B and D) with diameters of about 10 nm are distributed on the (210) crystal plane. This also confirms that the (210) crystal plane of brookite TiO_2 nanorods provides reduction sites for depositing noble metals. The loaded AuAg nanoparticles on brookite TiO_2 nanorods were further confirmed by EELS (Fig. 2F). It can be seen that Au and Ag have a fitted distribution on the characteristic nanorod

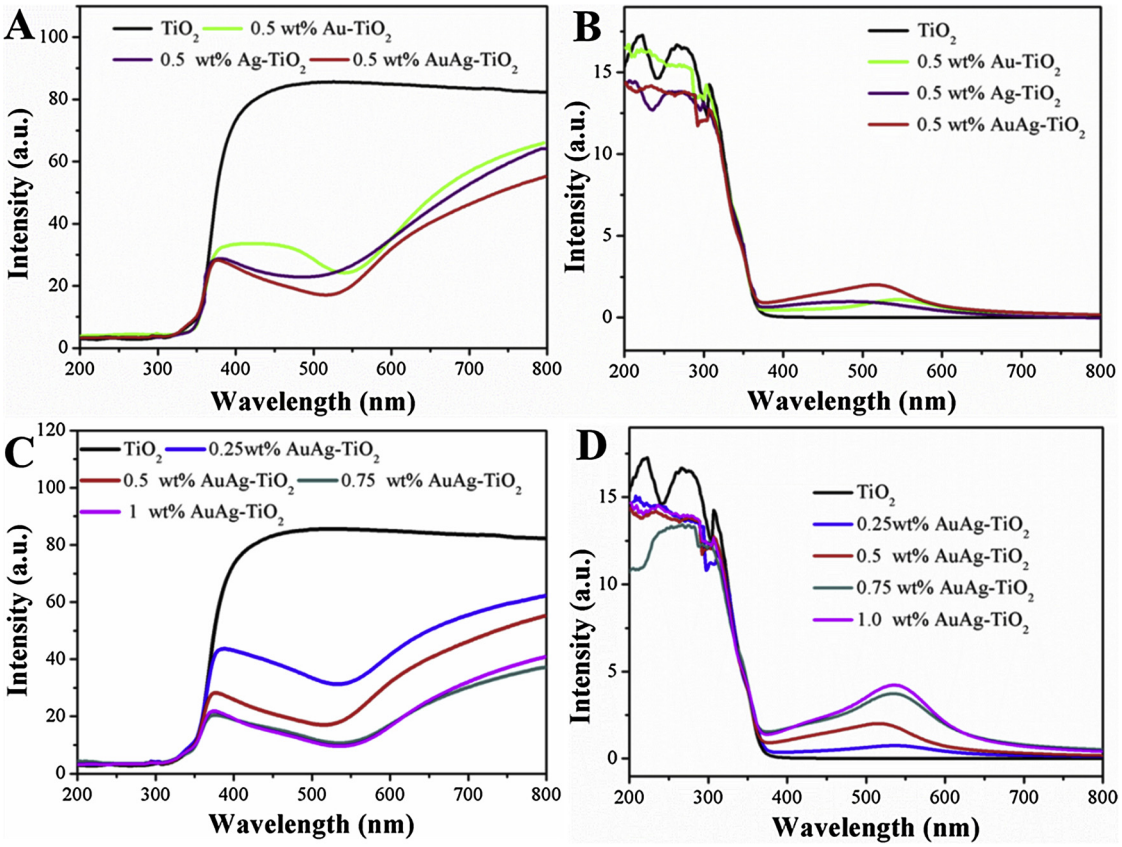

Fig. 5. UV–vis diffuse reflectance (DR) spectra (A) and UV–vis absorption spectra (B) of brookite TiO_2 and brookite TiO_2 loaded with 0.5 wt% of different metals and UV–vis DR (C) and UV–vis absorption spectra (D) of brookite TiO_2 and AuAg-TiO_2 with different loading amounts of AuAg.

Table 1
BET surface areas of the samples.

Samples	Commercial TiO_2	Brookite TiO_2	0.25 wt %AuAg-TiO_2	0.5 wt %AuAg-TiO_2	0.75 wt %AuAg-TiO_2	1.0 wt %AuAg-TiO_2
BET (m^2/g)	38.1	77.3	77.2	75.9	73.8	72.1

shape of TiO_2, demonstrating that the AuAg bimetallic nanoparticles have been successfully located on the as-prepared TiO_2 nanorods.

The loading amount of AuAg on brookite TiO_2 nanorods can be theoretically regulated by controlling the volume of the precursor solution. With an increase in the loading amount of AuAg, the nanoparticles become more obvious in SEM images. As depicted, The AuAg nanoparticles can hardly be seen in 0.25 wt% AuAg-TiO_2 nanorods (Fig. 3A) due to the relatively small loading amount. When the weight percentage of AuAg was increased to 0.5 wt%, a small amount of nanoparticles was distributed on the TiO_2 nanorods (Fig. 1D). However, a large amount of nanoparticles was deposited on the nanorods for 0.75 wt% AuAg-TiO_2 and 1.0 wt% AuAg-TiO_2 nanorods. It is notable that all of the nanoparticles were distributed on the reduction facets of nanorods, suggesting that the photoreduction reaction occurred on a specific crystal plane with separation of the reduction and oxidation sites in the brookite TiO_2 nanorods. For comparison, pure 0.5 wt% Au-loaded brookite TiO_2 and 0.5 wt% Ag-loaded brookite TiO_2 nanorods were synthesized, and SEM images are shown in Fig. 3. As in the case of 0.5 wt% AuAg-TiO_2, the Au-TiO_2 and Ag-TiO_2 nanorods had few nanoparticles on the reduction crystal planes of the nanorods. It was confirmed that pristine Au nanoparticles and Ag nanoparticles can be formed by photoreduction. For comparison, the SEM image of commercial brookite was also characterized. It is observed that commercial brookite is composed of stacked nanoparticles with diameter of nearly 20 nm.

The XRD patterns were characterized and are shown in Fig. 4, revealing the crystalline structure and crystal phase of samples. The peaks of pure nanorods can be well indexed to brookite TiO_2 (JCPDS: 00-015-0875) [17,18] without other impurity peaks, indicating high purity. Furthermore, the samples with different loading amounts of AuAg exhibited peaks that agreed well with the pristine brookite TiO_2 nanorods and no peak of Au or Ag, which is thought to be due to the small amount and good dispersion of loaded metals on the brookite TiO_2 nanorods. Similarly, there was no sign of Au (JCPDS: 65–2870) and Ag (JCPDS: 65–2871) [19,20] in the as-prepared Au-TiO_2 and Ag-TiO_2 as shown in Fig. 4C and 4D.

The optical properties of TiO_2, Au-TiO_2, Ag-TiO_2 and AuAg-TiO_2 were revealed by the UV–vis DR and absorption spectra shown in Fig. 5. The pure brookite TiO_2 shows an absorption edge at 380 nm in the UV light region, suggesting that pure brookite TiO_2 nanorods can not be excited by visible light. However, Au-TiO_2 and Ag-TiO_2 show absorption peaks at 547 and 467 nm, respectively, which are assigned to the LSPR effect of Au and Ag on brookite TiO_2 [21–24]. It is worth notable that the AuAg-TiO_2 nanorods showed absorption in a wide range of 400–600 nm due to the LSPR effect of both Au and Ag nanoparticles. This also implies that Au and Ag have a synergistic effect of LSPR for brookite TiO_2 nanorods and greatly improve the visible-light absorptivity. Moreover, visible-light absorption is enhanced with an increase in the loading amount of AuAg nanoparticles. Table 1 shows the BET surface areas of the as-prepared samples. The commercial brookite samples present surface area of 38.1 $m^2\,g^{-1}$, which is much smaller than that of as-prepared brookite TiO_2 nanorods. It can be seen that brookite TiO_2 nanorods had a surface area of 77.3 $m^2\,g^{-1}$, which provides numerous active sites for loading the AuAg bimetallic nanoparticles and photocatalytic reaction. Moreover, the surface area of the

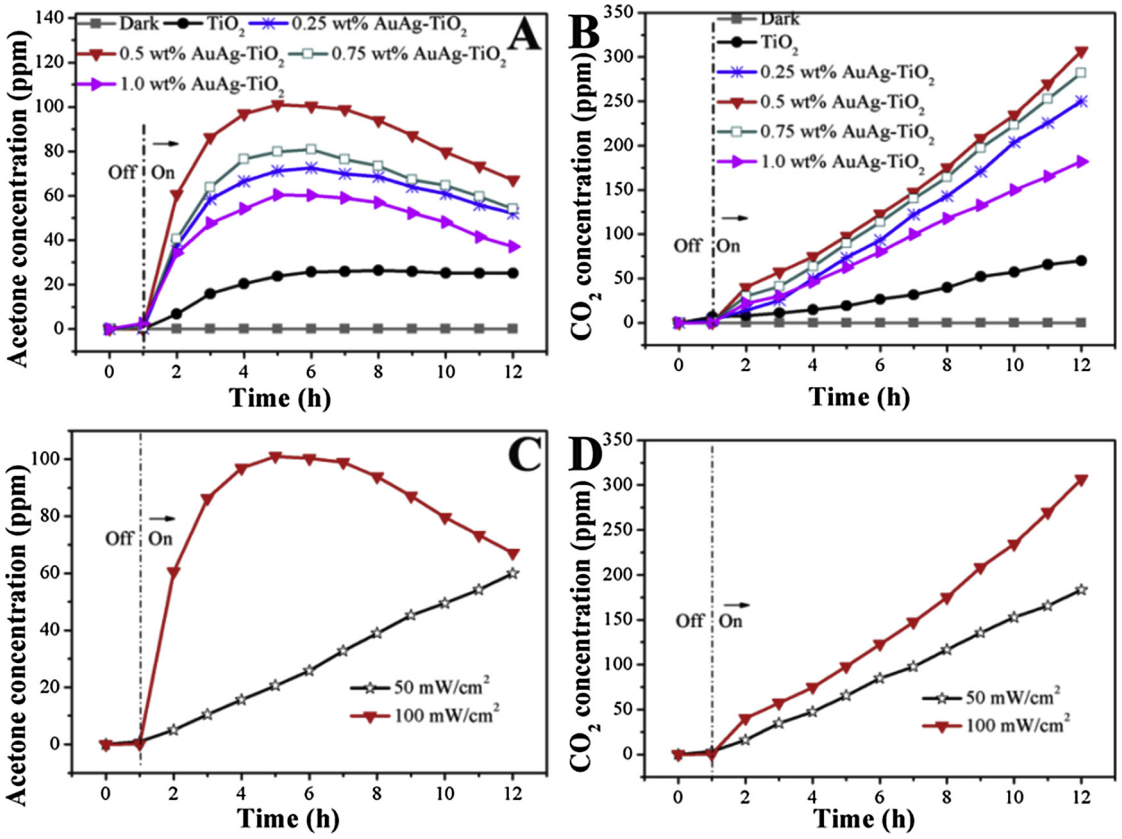

Fig. 6. Time courses of (A) acetone evolution and (B) CO_2 evolution from different photocatalysts and time courses of (C) acetone evolution and (D) CO_2 evolution from the 0.5 wt% AuAg-brookite TiO_2 under visible light with different light intensities.

samples showed a slight decrease with an increase in the loading amount of AuAg nanoparticles.

To demonstrate the LSPR effect of AuAg bimetallic nanoparticles on the reduction facets of brookite TiO_2 nanorods, the photocatalytic activities of pristine brookite TiO_2 nanorods and AuAg-brookite TiO_2 nanorods for oxidation of 2-propanol were evaluated. Fig. 6A and B show the time courses of acetone evolution and CO_2 evolution from different photocatalysts under visible light illumination ($440 < \lambda < 800$ nm). It can be clearly seen that the brookite TiO_2 nanorods exhibited a weak visible-light-driven response and almost no photocatalytic performance under dark conditions. The weak visible-light-driven response is thought to be resulted from the defects in the as-obtained brookite TiO_2 nanorods. Both surface and bulk oxygen vacancies would have functions in the photo-reaction process. Light absorption of photocatalysts can be improved by surface and bulk oxygen vacancies. Furthermore, the surface oxygen vacancies promote charge separation, while the bulk vacancies act as recombination center of photogenerated electrons and holes [25,26]. As characterized by the UV–vis absorption spectra (Fig. 5B), the as-prepared brookite TiO_2 shows no visible light absorption, indicating that the weak visible-light-driven photocatalytic response is mainly originated from the surface vacancies.

After loading AuAg bimetallic nanoparticles on the brookite TiO_2 nanorods, the photocatalytic properties were remarkably improved. The 0.5 wt% AuAg-TiO_2 nanorods showed the highest photocatalytic activity among the AuAg-loaded brookite TiO_2 nanorods tested, yielding 102 ppm of acetone when irradiated for 5 h with visible light. It is notable that the yield of acetone increased almost linearly over the 5-h period and then decreased due to the saturation of acetone on the surface of the photoatalysts and the decomposition from acetone to the final product, CO_2 [27]. However, the acetone production of brookite TiO_2 nanorods is only 25 ppm even irradiated by visible light for 5 h. Similarly, the 0.5 wt% AuAg-TiO_2 nanorods showed the highest level of CO_2 production during the photocatalytic process. Based on these results, it was concluded that the amount of AuAg nanoparticles has an important effect on the surface plasmon-induced photocatalytic activity.

In addition, the photocatalytic activity of AuAg-TiO_2 was found to be strongly dependent on the light intensity as shown in Fig. 6C and D. The acetone evolution in the case of illumination by visible light with intensity of 50 mW cm^{-2} showed a linear increase with extension of time to 12 h, indicating that the yield of acetone did not reach saturation during the photocatalytic process. In contrast, the saturated production of acetone can be obtained at 6 h in the case of 100 mW cm^{-2} visible light irradiation. However, it is should be noted that the CO_2 production over the 12-h period showed a linear increase with an increase of visible light intensity. The results suggested that the photocatalytic performance is triggered by photocatalytic oxidation over AuAg nanoparticles or the thermal effect related to photoabsorption of incident light.

An action spectrum was obtained to reveal the factor determining the photocatalytic reaction and LSPR induced visible light responsibility of AuAg-TiO_2 nanorods. An AQE plot (Fig. 7A) of AuAg-TiO_2 corresponds well to the Kubelka-Munk function, indicating that the photocatalytic behavior is induced by photoabsorption based on the LSPR effect of Au and Ag nanoparticles [28]. For comparison, the photocatalytic properties of pure Ag-TiO_2 and Au-TiO_2 were investigated to confirm the superiority of AuAg bimetallic nanoparticles. As demonstrated in Fig. 7B and C, 0.5 wt% AuAg-TiO_2 showed remarkably higher production levels of acetone and CO_2 than those of 0.5 wt% Au-TiO_2 and 0.5 wt% Ag-TiO_2. Moreover, the Au-TiO_2 nanorods showed the lowest photocatalytic activity among the samples tested, indicating a weak LSPR effect of Au nanoparticles on photocatalytic performance [29]. The acetone production derived by 0.5 wt%

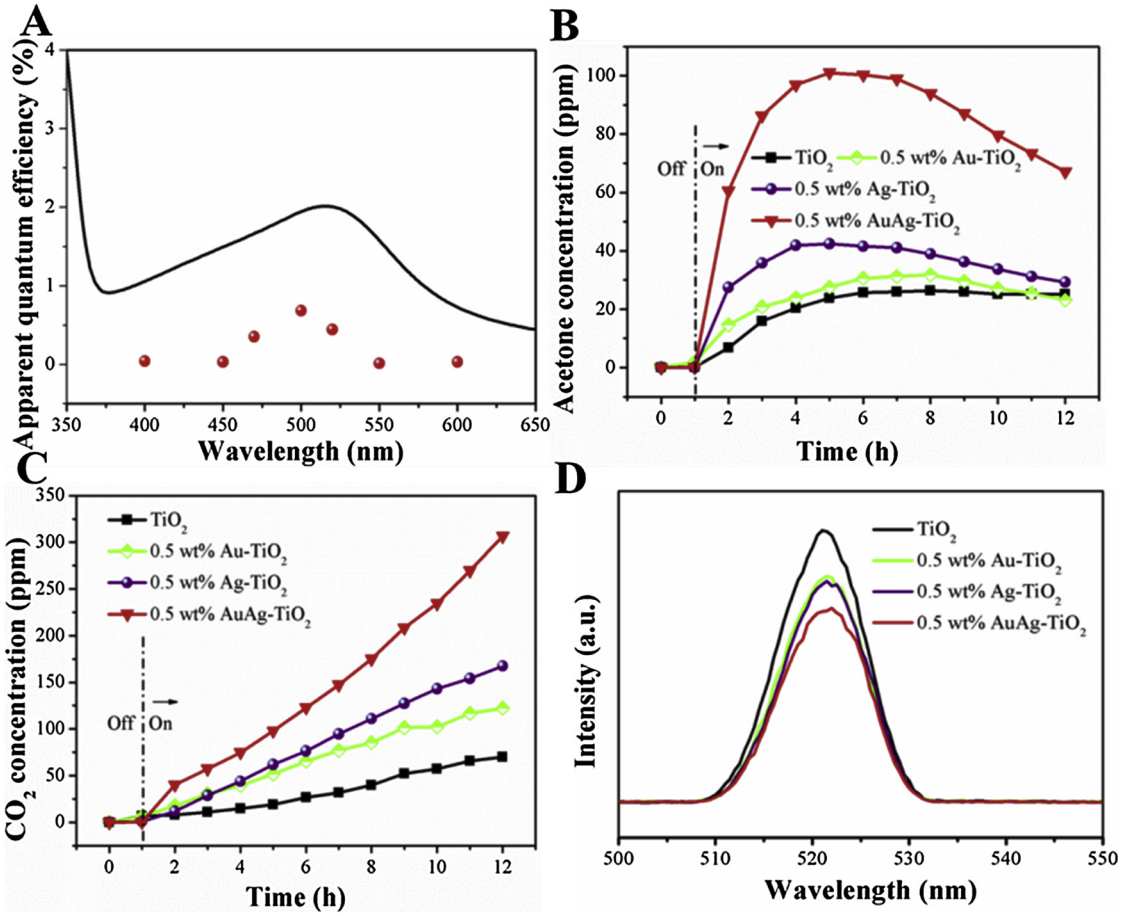

Fig. 7. (A) Action spectrum of acetone evolution from 2-propanol decomposition over 0.5 wt% AuAg-brookite TiO_2 nanorods together with Kubelka-Munk functions, time courses of (B) acetone evolution and (C) CO_2 evolution from Ag-TiO_2, Au-TiO_2 and AuAg-TiO_2 and (D) photoluminescence (PL) spectra of samples.

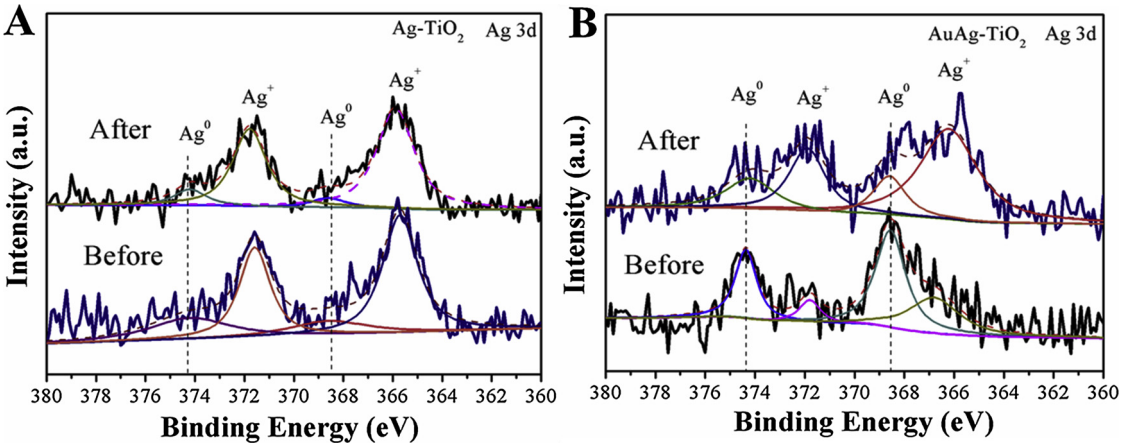

Fig. 8. 3d XPS patterns of (A) 0.5 wt% Ag-brookite TiO_2 and (B) 0.5 wt% AuAg-brookite TiO_2 before and after the photodecomposition process.

AuAg-TiO_2 is about 3 and 4 times of those of 0.5 wt% Ag-TiO_2 and 0.5 wt% Au-TiO_2, respectively. It has been proposed that the introduction of Au into Ag can greatly enhance the stability of Ag nanoparticles as well as preserve the high activity, which would provide an excellent LSPR effect [30].

Besides the enhanced visible light absorption of AuAg-TiO_2 verified by UV–vis absorption spectra, the PL intensities (Fig. 7D) of TiO_2 and metal loaded TiO_2 were measured to investigate the charge separation efficiency. The PL emission located at about 520 nm corresponds to the charge transfer transition of trapped electrons in oxygen vacancy and plasma particles [31,32]. As the PL emission is a result of recombination of electrons and holes, the quenching of photoluminescence validates the efficient charge separation. It is well observed that the modified brookite TiO_2 nanorods exhibit decreased PL peak intensity, confirming enhanced charge separation by metal deposition. More specifically, 0.5 wt% AuAg-TiO_2 nanorods showed higher charge separation efficiency than those of TiO_2, Au-TiO_2 and Ag-TiO_2 samples being consistent with the excellent photocatalytic performance under visible light irradiation. Moreover, Au-TiO_2 showed a much higher recombination rate of electrons and holes than that of Ag-TiO_2, indicating a weaker LSPR effect of Au nanoparticles than that of Ag nanoparticles on brookite TiO_2 nanorods. Based on these result, it is

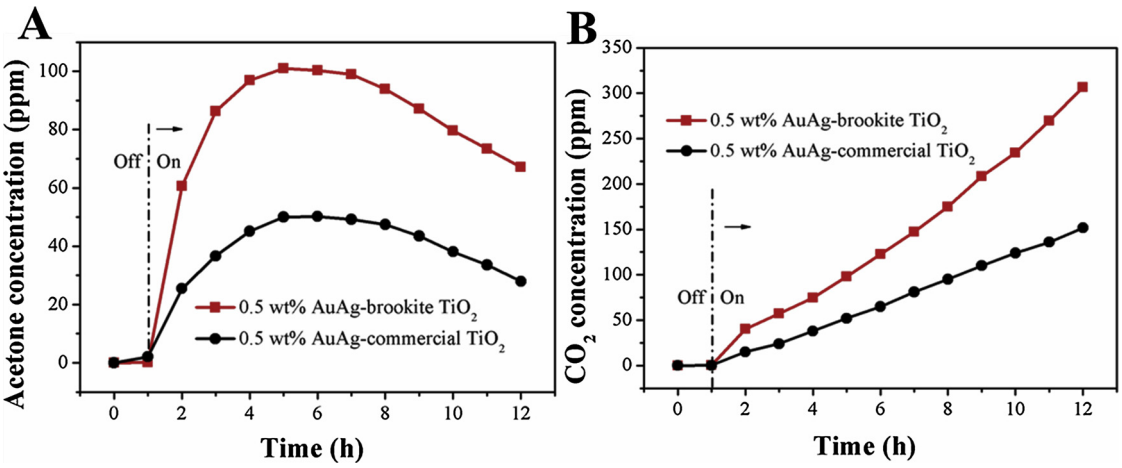

Fig. 9. Time courses of (A) acetone evolution and (B) CO_2 evolution derived from AuAg-commercial TiO_2 and AuAg-brookite TiO_2.

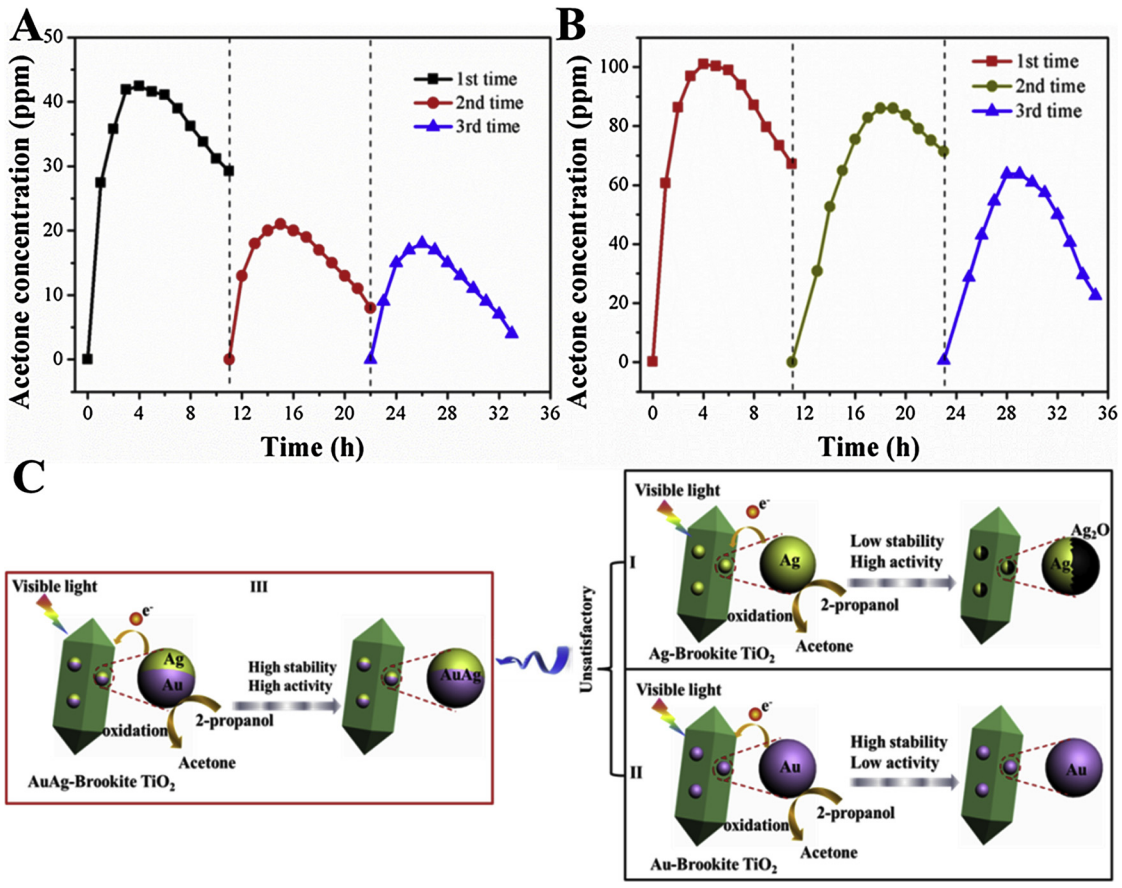

Fig. 10. Cyclic performance of (A) 0.5 wt% Ag-TiO_2 nanorods and (B) 0.5 wt% AuAg-TiO_2 nanorods for acetone production under visible light irradiation (C) illustration scheme for characteristics of as-prepared photocatalysts.

concluded that the combination of Au and Ag could provide a strong LSPR effect as well as stable Ag under visible light illumination, enabling the transfer of excited electrons from AuAg nanoparticles to the conduction band of TiO_2. As a result, the charge separation of AuAg-TiO_2 was greatly enhanced, being closely related to the photocatalytic activity.

In order to confirm the valence states of Ag, XPS measurements were performed on Ag-TiO_2 and 0.5 wt% AuAg-TiO_2 before and after photocatalytic tests (Fig. 8). For 0.5 wt% Ag-TiO_2 nanorods, the Ag 3d XPS pattern showed binding energies of Ag at 374.2 eV and 368.6 eV and binding energies of Ag^+ at 365.8 eV and 371.8 eV, confirming the co-existence of Ag and Ag_2O [27,33]. Furthermore, the binding energy peak of Ag^+ was much higher than that of Ag, suggesting that Ag had been greatly oxidized before utilization. After photodecomposition, the peaks of Ag decreased and the binding energies of Ag $3d_{5/2}$ and Ag $3d_{3/2}$ of Ag^+ at 365.8 eV and 371.8 eV in the 3d XPS pattern exhibit strong intensities, indicating that the pure Ag nanoparticles were highly unstable and oxidized during the photocatalytic process. However, the Ag 3d XPS spectra of 0.5 wt% AuAg-TiO_2 nanorods showed great differences from those of 0.5 wt% Ag-TiO_2. The Ag 3d XPS pattern of 0.5 wt% AuAg-TiO_2 before the photocatalytic test showed strong peaks of Ag at about 374.2 eV and 368.6 eV and weak peaks of Ag^+, suggesting that

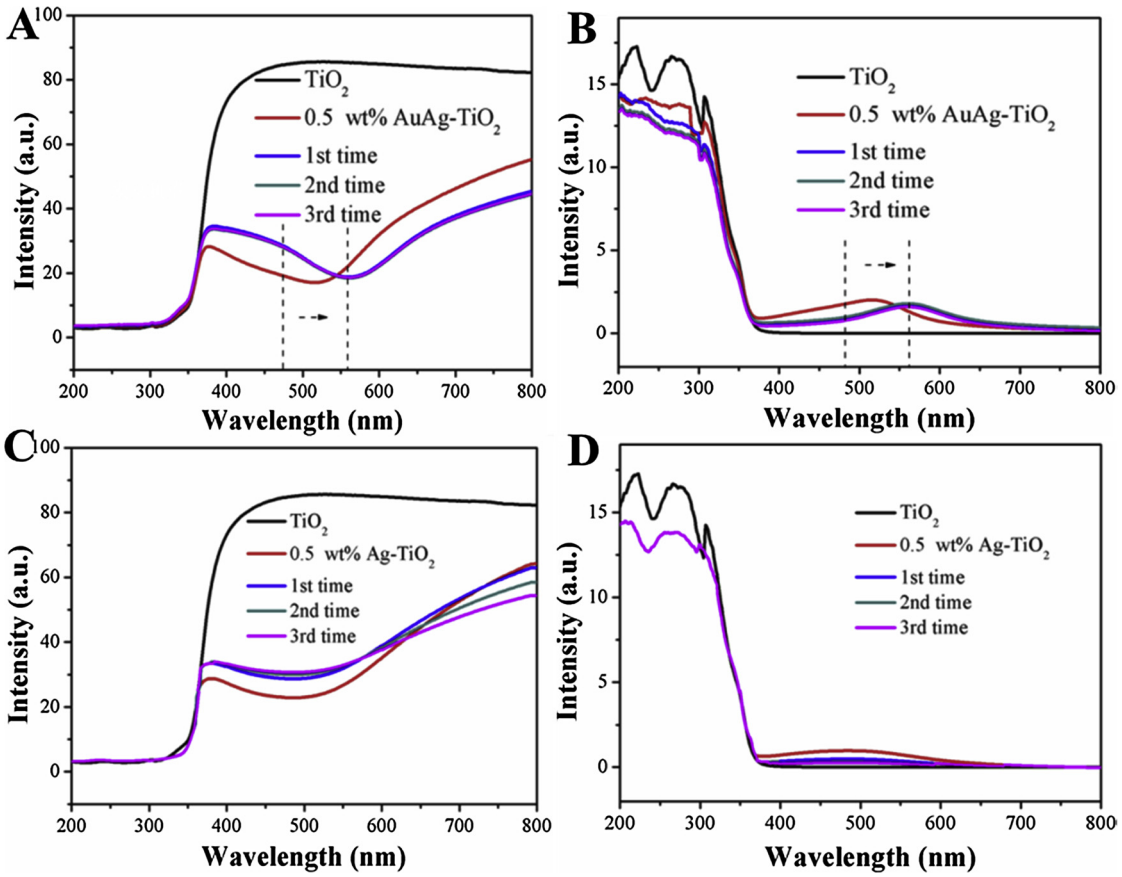

Fig. 11. UV–vis DR spectra (A) and UV–vis absorption spectra (B) of AuAg-TiO_2 with 3 photocatalytic tests and UV–vis DR spectra (C) and UV–vis absorption spectra (D) of Ag-TiO_2 with 3 photocatalytic tests.

AuAg bimetallic metals benefit the stability of Ag. On the other hand, the binding energy peak of Ag^+ increased greatly after the photocatalytic test, indicating that Ag was partially oxidized during the photocatalytic reaction [34]. These results suggest that Ag is easily oxidized in the process of photocatalytic reaction.

Apart from the advantages of AuAg bimetallic nanoparticles, control of the morphology of brookite TiO_2 nanorods contributes to the high photocatalytic performance, as was confirmed by a comparison of photocatalytic activities of 0.5 wt% AuAg-brookite TiO_2 and 0.5 wt% AuAg-commercial brookite TiO_2 (Fig. 9). It should be mentioned that the production levels of acetone and CO_2 derived from the AuAg-commercial brookite TiO_2 were only about half of those generated over AuAg-brookite TiO_2. It is thought that selective loading of AuAg bimetallic nanoparticles on the reduction sites of brookite TiO_2 effectively promote charge separation and the large surface area of brookite nanorods (Table 1) furnishes numerous active sites, which are responsible for the superior photocatalytic activity. More specifically, the photogenerated electrons are transferred from AuAg nanoparticles to the reduction sites of brookite TiO_2 nanorods and take part in the reduction process, decreasing the recombination of electrons and holes. However, AuAg nanoparticles are deposited randomly on commercial brookite TiO_2 particle and then the photogenerated electrons move from AuAg to brookite TiO_2 under visible-light irradiation. The mixed electrons and holes in AuAg-commercial TiO_2 would increase the recombination rate, leading to low photocatalytic activity.

The cycling stabilities of the 0.5 wt% Ag-TiO_2 nanorods and 0.5 wt% AuAg-TiO_2 are shown in Fig. 10. Cycling stability is an important factor for practical applications of photocatalysts. Notably, acetone evolution from 0.5 wt% Ag-TiO_2 showed a significant decrease at the second photocatalytic application compared to that in the initial photocatalytic test. Moreover, a comparison of the decay efficiencies of photocatalytic activity of AuAg-TiO_2 and Ag-TiO_2 confirmed the superiority of AuAg-loaded brookite TiO_2 nanorods. After 3 cycles, the photocatalytic efficiency of 0.5 wt% Ag-TiO_2 had decreased to 41.2% of that in the initial test. However, the acetone production over 0.5 wt% AuAg-TiO_2 nanorods was as high as 64 ppm at 5 h after 3 cycles, which was 62.7% of the initial production, indicating that AuAg bimetallic nanoparticles are effective and stable during the photocatalytic reaction [35]. Based on the above results, it can be concluded that the introduction of Au into Ag nanoparticles effectively enhances the photocatalytic stability. As shown in Fig. 10C, Ag and Au nanoparticles provide photogenerated electrons to brookite TiO_2 under visible light. The photogenerated electrons directly participate in the reduction reaction and the holes left in the metals participate in the oxidation reaction, enabling efficient charge separation. Since the Ag nanoparticles are easily to be oxidized to Ag_2O during the photocatalytic process, the photocatalytic stability of Ag-TiO_2 is unsatisfactory. As Au nanoparticles have good stability and a weak LSPR effect, the combination of Au and Ag would provide good stability and a high level of activity.

UV-visible DR and absorption spectra (Fig. 11) of AuAg-TiO_2 and Ag-TiO_2 after photocatalytic cycling tests were obtained to confirm the aforementioned proposal. For AuAg-TiO_2, the absorption peak showed a red shift in the first photocatalytic test and almost no change in the second and third photocatalytic tests. The obvious red-shift of absorption peak is proposed to be devoted to the partial oxidation of Ag during the photocatalytic reaction, which has been confirmed by the Ag 3d XPS pattern as shown in Fig. 8. Importantly, the intensity of the absorption peak derived from the LSPR effect showed a slight decrease after photocatalytic cycling characterization that is related to the good photocatalytic stability. However, the LSPR effect of Ag-TiO_2 showed a significant decrease after the photocatalytic process, corresponding to the oxidation of Ag nanoparticles. After 3 photocatalytic tests, Ag in

TiO_2-Ag has bad been greatly oxidized due to the weak absorption in the visible light range, being consistent with the low level of photocatalytic activity. It was confirmed that the design of AuAg nanoparticles could effectively facilitate the stability of Ag nanoparticles and high photocatalytic performance.

4. Conclusion

In summary, AuAg nanoparticles were photoreduced on the reduction crystal planes of brookite TiO_2 nanorods, greatly promoting visible-light-induced photocatalytic activities. The selectively deposited AuAg bimetallic nanoparticles provide not only a strong LSPR effect but also good stability, resulting in excellent photocatalytic performance of AuAg-TiO_2 nanorods for decomposition of 2-propanol. By regulating the amount of loaded AuAg nanoparticles, a significantly high level of photocatalytic activity could be obtained by 0.5 wt% AuAg-TiO_2 nanorods. This strategy offers an effective method for developing visible-light-responsive photocatalysts as well as for investigating the LSPR effect of AuAg bimetallic nanoparticles on brookite TiO_2 nanorods.

References

[1] L.X. Zheng, S.C. Han, H. Liu, P.P. Yu, X.S. Fang, Hierarchical MoS_2nanosheet@TiO_2nanotube array composites with enhanced photocatalytic and photocurrent performances, Small 12 (2016) 1527–1536, https://doi.org/10.1002/smll.201503441.

[2] F. Iskandar, A.B.D. Nandiyanto, K.M. Yun, C.J. Hogan, J.K. Okuyama, P. Biswas, Enhanced photocatalytic performance of brookite TiO_2 macroporous particles prepared by spray drying with colloidal templating, Adv. Mater. 19 (2007) 1408–1412, https://doi.org/10.1002/adma.200601822.

[3] K. Maeda, N. Murakami, T. Ohno, Dependence of activity of rutile titanium(IV) oxide powder for photocatalytic overall water splitting on structural properties, J. Phys. Chem. C 118 (2014) 9093–9100, https://doi.org/10.1021/jp502949q.

[4] J.J.M. Vequizo, H. Matsunaga, T. Ishiku, S. Kamimura, T. Ohno, A. Yamakata, Trapping-induced enhancement of photocatalytic activity on brookite TiO_2powders: comparison with anatase and rutile TiO_2powders, ACS Catal. 7 (2017) 2644–2651, https://doi.org/10.1021/acscatal.7b00131.

[5] L.J. Liu, H.L. Zhao, J.M. Andino, Y. Li, Photocatalytic CO2reduction with H2O on TiO2nanocrystals: comparison of anatase, rutile, and brookite polymorphs and exploration of surface chemistry, ACS Catal. 2 (2012) 1817–1828, https://doi.org/10.1021/cs300273q.

[6] J.F. Zhang, P. Zhou, J.J. Liu, J.G. Yu, New understanding of the difference of photocatalytic activity among anatase, rutile and brookite TiO_2, Phys. Chem. Chem. Phys. 16 (2014) 20382–20386 https://pubs.rsc.org/en/content/articlelanding/2014/cp/c4cp02201g.

[7] K. Li, B.S. Peng, J.P. Jin, L. Zan, T.Y. Peng, Carbon nitride nanodots decorated brookite TiO_2 quasi nanocubes for enhanced activity and selectivity of visible-light-driven CO_2 reduction, Appl. Catal. B: Environ. 203 (2017) 910–916, https://doi.org/10.1016/j.apcatb.2016.11.001.

[8] M.X. Xu, Y.H. Wang, J.F. Geng, D.W. Jing, Photodecomposition of NOx on Ag/TiO_2composite catalysts in a gas phase reactor, Chem. Eng. J. 307 (2017) 181–188, https://doi.org/10.1016/j.cej.2016.08.080.

[9] K.K. Paul, P.K. Giri, Role of surface plasmons and hot electrons on the multi-step photocatalytic decay by defect enriched Ag@TiO_2nanorods under visible light, J. Phys. Chem. C 121 (2017) 20016–20030, https://doi.org/10.1021/acs.jpcc.7b05328.

[10] M. Zhao, H. Xu, S.X. Quyang, H. Tong, H.Y. Chen, Y.X. Li, L.Z. Song, J.H. Ye, Fabricating a Au@TiO_2plasmonic system to elucidate alkali-induced enhancement of photocatalytic H_2evolution: surface potential shift or methanol oxidation acceleration, ACS Catal. 8 (2018) 4266–4277, https://doi.org/10.1021/acscatal.8b00317.

[11] H.L. Ran, J.J. Fan, X.L. Zhang, J. Mao, G.S. Shao, Enhanced performances of dye-sensitized solar cells based on Au-TiO_2 and Ag-TiO_2 plasmonic hybrid nanocomposites, Appl. Surf. Sci. 430 (2018) 415–423, https://doi.org/10.1016/j.apsusc.2017.07.107.

[12] M. Tahir, B. Tahir, N.A.S. Amin, Synergistic effect in plasmonic Au/Ag alloy NPs co-coated TiO_2NWs toward visible-light enhanced CO_2 photoreduction to fuels, Appl. Catal. B: Environ. 204 (2017) 548–560, https://doi.org/10.1016/j.apcatb.2016.11.062.

[13] S.P. Lim, Y.S. Lim, A. Pandikumar, H.N. Lim, Y.H. Ng, R. Ramaraj, D.C.S. Bien, Q.K. Abou-Zied, N.M. Huang, Gold–silver@TiO_2 nanocomposite-modified plasmonic photoanodes for higher efficiency dye-sensitized solar cells, Phys. Chem. Chem. Phys. 19 (2017) 1395–1407 https://pubs.rsc.org/en/content/articlelanding/2017/cp/c6cp05950c.

[14] T. Ohno, T. Higo, H. Saito, S.S. Yuajn, Z.Y. Jin, Y. Yang, T. Tsubota, Dependence of photocatalytic activity on aspect ratio of a brookite TiO_2 nanorod and drastic improvement in visible light responsibility of a brookite TiO_2 nanorod by site-selective modification of Fe^{3+} on exposed faces, J. Mol. Catal. A Chem. 396 (2015) 261–267, https://doi.org/10.1016/j.molcata.2014.09.036.

[15] T. Ohno, T. Higo, N. Murakami, H. Saito, Q.T. Zhang, Y. Yang, T. Tsubota, Photocatalytic reduction of CO_2 over exposed-crystal-face-controlled TiO_2 nanorod having a brookite phase with co-catalyst loading, Appl. Catal. B: Environ. 152—153 (2014) 309–316, https://doi.org/10.1016/j.apcatb.2014.01.048.

[16] M. Choi, J.H. Lim, M. Baek, W. Choi, W. Kim, K. Yong, Investigating the unrevealed photocatalytic activity and stability of nanostructured brookite TiO_2film as an environmental photocatalyst, ACS Appl. Mater. Interfaces 9 (2017) 16252–16260, https://doi.org/10.1021/acsami.7b03481.

[17] M. Bellardita, A.D. Paola, B. Megna, L. Palmisano, Absolute crystallinity and photocatalytic activity of brookite TiO_2 samples, Appl. Catal. B: Environ. 201 (2017) 150–158, https://doi.org/10.1016/j.apcatb.2016.08.012.

[18] S.Y. Lim, T.S. Su, T.Y. Hsieh, P.C. Lo, T.C. Wei, Beyond langevin recombination: how equilibrium between free carriers and charge transfer states determines the open-circuit voltage of organic solar cells, Adv. Energy Mater. (2017), https://doi.org/10.1002/aenm.201500123 1700169.

[19] C.B. Gao, Y.X. Hu, M.S. Wang, M.F. Chi, Y.D. Yin, Fully alloyed Ag/Au nanospheres: combining the plasmonic property of Ag with the stability of Au, J. Am. Chem. Soc. 136 (2014) 7474–7479, https://doi.org/10.1021/ja502890c.

[20] D.Q. Zhang, M.C. Wen, S.S. Zhang, P.J. Liu, W. Zhu, Au nanoparticles enhanced rutile TiO_2 nanorod bundles with high visible-light photocatalytic performance for NO oxidation, Appl. Catal. B: Environ. 147 (2014) 610–616, https://doi.org/10.1016/j.apcatb.2013.09.042.

[21] H.M. Chen, C.K. Chen, M.L. Tseng, P.C. Wu, C.M. Chang, L.C. Cheng, H.W. Huang, T.S. Chan, D.W. Huang, R.S. Liu, D.P. Tsai, Plasmonic ZnO/Ag embedded structures as collecting layers for photogenerating electrons in solar hydrogen generation photoelectrodes, Small 17 (2013) 2926–2936, https://doi.org/10.1002/smll.201202547.

[22] R. Solarska, K. Bienkowski, S. Zoladek, A. Majcher, T. Stefaniuk, P.J. Kulesza, J. Augustynski, Enhanced water splitting at thin film tungsten trioxide photoanodes bearing plasmonic gold–polyoxometalate particles, Angew. Chem. Int. Ed. 53 (2014) 14196–14200, https://doi.org/10.1002/anie.201408374.

[23] M. Valenti, D. Dolat, G. Biskos, A. Schmidt-Ott, W.A. Smith, Enhancement of the photoelectrochemical performance of $CuWO_4$thin films for solar water splitting by plasmonic nanoparticle functionalization, J. Phys. Chem. C 119 (2015) 2096–2104, https://doi.org/10.1021/jp506349t.

[24] H. Wang, T.T. You, W.W. Shi, J.H. Li, L. Guo, Au/TiO_2/Au as a plasmonic coupling photocatalyst, J. Phys. Chem. C 116 (2012) 6490–6494, https://doi.org/10.1021/jp212303q.

[25] H. Zhang, J.M. Cai, Y.T. Wang, M.Q. Wu, M. Meng, Y. Tian, X.G. Li, J. Zhang, L.R. Zheng, Z. Jiang, J.L. Gong, Insights into the effects of surface/bulk defects on photocatalytic hydrogen evolution over TiO_2 with exposed {001} facets, Appl. Catal. B: Environ. 220 (2018) 126–136, https://doi.org/10.1016/j.apcatb.2017.08.046.

[26] J.L. Li, M. Zhang, Z.J. Guan, Q.Y. Li, C.Q. He, J.J. Yang, Appl. Catal. B: Environ. 206 (2017) 300–307, https://doi.org/10.1016/j.apcatb.2017.01.025.

[27] S. Kamimura, S. Yamashita, S. Abe, T. Tsubota, T. Ohno, Effect of core@shell (Au@Ag) nanostructure on surface plasmon-induced photocatalytic activity under visible light irradiation, Appl. Catal. B: Environ. 211 (2017) 11–17, https://doi.org/10.1016/j.apcatb.2017.04.028.

[28] M. Ou, S.P. Wan, Q. Zhong, S.L. Zhang, Y. Song, L.N. Guo, W. Cai, Y.L. Xu, Hierarchical Z-scheme photocatalyst of g-C_3N_4@Ag/$BiVO_4$(040) with enhanced visible-light-induced photocatalytic oxidation performance, Appl. Catal. B: Environ. 221 (2018) 97–107, https://doi.org/10.1016/j.apcatb.2017.09.005.

[29] N. Zhou, L. Polavarapu, N. Gao, Y.L. Pan, P.Y. Yuan, Q. Wang, Q.H. Xu, TiO_2 coated Au/Ag nanorods with enhanced photocatalytic activity under visible light irradiation, Nanoscale 5 (2013) 4236–4241 https://pubs.rsc.org/en/content/articlelanding/2013/nr/c3nr00517h.

[30] A. Tanaka, K. Hashimoto, H. Kominami, A very simple method for the preparation of Au/TiO_2 plasmonic photocatalysts working under irradiation of visible light in the range of 600–700 nm, Chem. Commun. 53 (2017) 4759–4762 https://pubs.rsc.org/en/content/articlelanding/2017/cc/c7cc01444a.

[31] L.G. Devi, B. Nagaraj, K.E. Rajashekhar, Synergistic effect of Ag deposition and nitrogen doping in TiO_2 for the degradation of phenol under solar irradiation in presence of electron acceptor, Chem. Eng. J. 181-182 (2012) 259–266, https://doi.org/10.1016/j.cej.2011.11.076.

[32] T. Harifi, M. Montazer, Fe^{3+}:Ag/TiO_2 nanocomposite: synthesis, characterization and photocatalytic activity under UV and visible light irradiation, Appl. Catal. A Gen. 473 (2014) 104–115, https://doi.org/10.1016/j.apcata.2014.01.005.

[33] A. Tanaka, K. Hashimoto, H. Kominami, Control of surface plasmon resonance of Au/SnO_2 by modification with Ag and Cu for photoinduced reactions under visible-light irradiation over a wide range, Chem. Eur. J. 22 (2016) 4592–4599, https://doi.org/10.1002/chem.201504606.

[34] H. Li, Y. Sun, Z.Y. Yuan, Y.P. Zhu, T.Y. Ma, Titanium phosphonate based metal–organic frameworks with hierarchical porosity for enhanced photocatalytic hydrogen evolution, Angew. Chem. Int. Ed. 57 (2018) 3222–3227, https://doi.org/10.1002/anie.201712925.

[35] N. Shao, J.N. Wang, D.D. Wang, P. Corvini, Preparation of three-dimensional Ag_3PO_4/TiO_2@MoS_2 for enhanced visible-light photocatalytic activity and anti-photocorrosion, Appl. Catal. B: Environ. 203 (2017), https://doi.org/10.1016/j.apcatb.2016.11.008 984–978.